Monthly Notices
of the
ROYAL ASTRONOMICAL SOCIETY

Mon. Not. R. Astron. Soc. **414,** 3434–3443 (2011) doi:10.1111/j.1365-2966.2011.18645.x

Fortnightly fluctuations in the O−C diagram of CS 1246★

B. N. Barlow,[1]†‡ B. H. Dunlap,[1]‡ J. C. Clemens,[1] D. E. Reichart,[2] K. M. Ivarsen,[2] A. P. LaCluyze,[2] J. B. Haislip[2] and M. C. Nysewander[3]

[1]*Department of Physics and Astronomy, University of North Carolina, Chapel Hill, NC 27599-3255, USA*
[2]*SKYNET, Department of Physics and Astronomy, University of North Carolina, Chapel Hill, NC 27599-3255, USA*
[3]*Alion Science & Technology, 1000 Park Forty Plaza, Durham, NC 27713, USA*

Accepted 2011 March 3. Received 2011 March 2; in original form 2010 September 28

ABSTRACT

Dominated by a single, large-amplitude pulsation mode, the rapidly pulsating hot subdwarf B star CS 1246 is a prime candidate for a long-term O−C diagram study. We collected nearly 400 h of photometry with the 0.41-m Panchromatic Robotic Optical Monitoring and Polarimetry Telescopes over a time-span of 14 months to begin looking for secular variations in the pulse timings. Interestingly, the O−C diagram is dominated by a strong sinusoidal pattern with a period of 14.1 d and an amplitude of 10.7 light-seconds. Underneath this sine wave is a secular trend implying a decrease in the 371.7-s pulsational period of $\dot{P} = -1.9 \times 10^{-11}$, which we attribute to the evolution of the star through the Hertzsprung–Russell diagram. The sinusoidal variation could be produced by the presence of a low-mass companion, with $m \sin i \simeq 0.12\,\mathrm{M}_{\odot}$, orbiting the subdwarf B star at a distance of 20 $\mathrm{R}_{\odot}$. An analysis of the combined light curve reveals the presence of a low-amplitude first harmonic to the main pulsation mode.

Key words: stars: individual: CS 1246 – stars: oscillations – subdwarfs.

1 HOT SUBDWARFS AS BINARY SYSTEMS

Subluminous B (sdB) stars represent one of the least-understood stages of stellar evolution, yet they dominate surveys of faint blue objects and are found in almost all Galactic stellar populations. They are the field counterparts of the extreme horizontal branch (EHB) stars in globular clusters and lie in a region of the Hertzsprung–Russell (H–R) diagram corresponding to the location of models with He-burning cores and extremely thin H envelopes (Heber 1986). Understanding these stars better would illuminate the enigmatic 'second-parameter' problem in globular cluster evolution, improve the synthesis modelling of the ultraviolet upturn in giant elliptical galaxies, identify the evolutionary mechanisms responsible for guiding main-sequence stars to this state and constrain the physical properties of the dense plasmas present in these compact objects.

Presumably, the sdB stars have been stripped of almost all their surface hydrogen after the red giant phase, but how and why this stripping occurs is still debated. Some have proposed binary models in which the extra angular momentum provided by a companion manages to expel almost all of the hydrogen envelope (Han et al. 2002, 2003). Others have proposed that more modest amounts of angular momentum, as might be resident in a planet, could accomplish the same effect (Soker 1998). Still, others are able to draw hot subdwarf stars from their models without the assistance of a companion (D'Cruz et al. 1996).

In any case, companions may be profoundly important for understanding the evolution of sdB stars, and placing constraints on the nature of these systems may shed light on their evolutionary histories. Several studies have shown an unusually high binary fraction amongst the hot subdwarf stars (Maxted et al. 2001; Napiwotzki et al. 2004). Measurements of radial velocity (RV) shifts have led to the orbital parameters of approximately 85 sdB binaries (see table A.1 from Geier et al. 2011). The periods of such systems range from 0.07 to 28 d, with a peak between 0.5 and 1.0 d. RV variability studies are most sensitive to systems with shorter periods and higher total masses, and as a result, few system parameters exist for longer period binaries. Only two systems with periods above 10 d have well-determined orbital parameters (PG 0850+170 and PG 1619+522; Morales-Rueda et al. 2003).

★Based on observations at the SOAR Telescope, a collaboration between CPNq-Brazil, NOAO, UNC and MSU, and on observations collected at the PROMPT array via SKYNET.

†E-mail: bbarlow@physics.unc.edu
‡Visiting Astronomer, CTIO, National Optical Astronomy Observatories, which are operated by the Association of Universities for Research in Astronomy, Inc., under contract with the National Science Foundation.

The discovery of the first of the pulsating sdB (sdBV[1]) stars (Kilkenny et al. 1997) in conjunction with the first sdBV models (Charpinet et al. 1996, 1997) opened the possibility of exploring their structure through a combination of spectral analysis and stellar seismology. Multicolour photometry and time-series spectroscopy techniques, for example, have revealed information about the total mass, envelope mass and chemical stratification for a handful of pulsators (see Østensen 2009 for a review). The pulsations may also provide the opportunity to detect companions by using phase measurements to look for oscillations in the arrival times of the pulses. Silvotti et al. (2007) used this method successfully to detect a $3.2M_{\rm Jup}$ planet around the star V391 Peg (HS 2201+2610). Their study also resulted in the first published measurement of $\dot{P}$ for a pulsating sdB star, constraining the evolutionary state of V391 Peg.

CS 1246, a recently discovered sdBV$_{\rm r}$ star (Barlow et al. 2010), is a prime target for an extended O−C diagram study since it exhibits a single, large-amplitude pulsation mode. Using the 0.41-m Panchromatic Robotic Optical Monitoring and Polarimetry Telescopes (PROMPT) array, we monitored the pulse timings for 14 months by collecting nearly 400 h of time-series photometry. The O−C diagram shows a sinusoidal oscillation superimposed on a parabola. We interpret the quadratic term as a secular decrease in the pulsation period, while the sinusoidal oscillation implies the presence of a low-mass stellar companion, probably an M dwarf or a white dwarf. Our study marks the second time $\dot{P}$ and the mass of a companion has been estimated for a hot subdwarf star using the O−C method.

2 PHOTOMETRIC DATA

We began monitoring CS 1246 in 2009 using the 0.41-m PROMPT on Cerro Tololo to look for phase variations in the pulsations. The PROMPT operate under the control of a prioritized, queue-scheduling system called SKYNET and are 100 per cent automated. Priority levels are assigned to all observations in the queue and, consequently, some of our photometry runs were interrupted by higher priority targets such as gamma-ray bursts. For additional details on the PROMPT and SKYNET, we refer the reader to Reichart et al. (2005).

Over the course of 14 months, we collected more than 33 000 individual frames representing 400 h of time-series photometry. The majority of these data were taken in a 4-month time-span between 2010 January and May with the PROMPT 3. On a typical night, we obtained at least 3 h of photometry with 30-s exposures and no filter; during these observations, our duty cycle was on average 83 per cent. We also include in this work the photometry from 2009 presented in Barlow et al. (2010) and a few light curves obtained with the Goodman Spectrograph (Clemens, Crain & Anderson 2004) on the 4.1-m SOAR telescope. Appendix A presents a detailed log of our photometric observations.

[1] Here we use the nomenclature proposed by Kilkenny et al. (2010). All sdB pulsators are given the basename 'sdBV'; the subscripts 'r' and 's' are added upon observations of rapid and slow pulsations, respectively. For reference, the sdBV$_{\rm r}$ stars have also been called V361 Hya and EC 14026 stars, while the sdBV$_{\rm s}$ stars have the aliases PG 1716, V1093 Her and 'Betsy' stars.

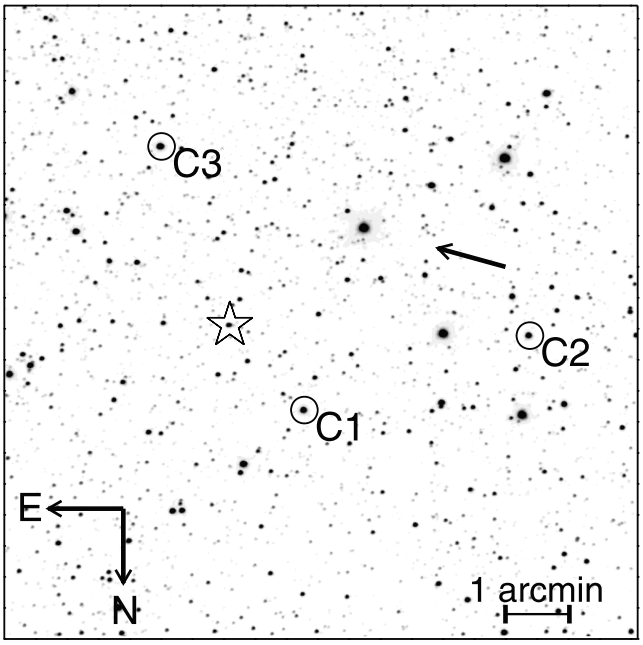

Figure 1. Field image of CS 1246. Image shown is a stack of 100 30-s open-filter frames taken with the PROMPT 3. CS 1246 is marked with a star symbol, while the comparison stars used for the majority of the light curves are labelled C1–C3. The arrow indicates the drift direction and magnitude of the field as it appears in the frames over 3 h of tracking with the PROMPT 3.

2.1 Reduction and analysis

Images were bias subtracted and flat-fielded in IRAF[2] using standard procedures. We then extracted our photometry using Antonio Kanaan's external IRAF package CCD_HSP. We chose aperture radii that maximized the signal-to-noise ratio in the nightly light curves and used sky annuli to estimate and subtract off counts from the sky. As the field is densely packed with stars, we were careful to avoid the contamination of the apertures and annuli from neighbouring stars. We removed sky transparency variations by dividing our light curves with those of constant comparison stars. Such stars were chosen by selecting from those in the field that were photometrically constant in time, not contaminated by nearby stars, substantially brighter than CS 1246, and not saturated during a 30-s exposure. Additionally, we avoided comparison stars that were likely to drift out of the frame during the PROMPT runs due to an approximately 0.4 arcmin h^{-1} tracking error in the mounts. These selection criteria provided us with three dependable comparison stars, as shown in the field image in Fig. 1. Finally, we fitted and normalized the light curves with parabolas to remove residual atmospheric extinction effects. This process can remove real variations in the stellar flux of the order of the run lengths, making it difficult to detect lower frequency g-mode oscillations, if they exist. All time-stamps were converted to a Barycentric Julian Ephemeris Date (BJED) using the WQED suite (v2.0; Thompson & Mullally 2009), which employs the method of Stumpff (1980).

We analysed our light curves with a combination of Fourier analysis and least-squares fits of sine waves, using both PERIOD04 (Lenz

[2] IRAF is distributed by the National Optical Astronomy Observatories, which are operated by the Association of Universities for Research in Astronomy, Inc., under cooperative agreement with the National Science Foundation.

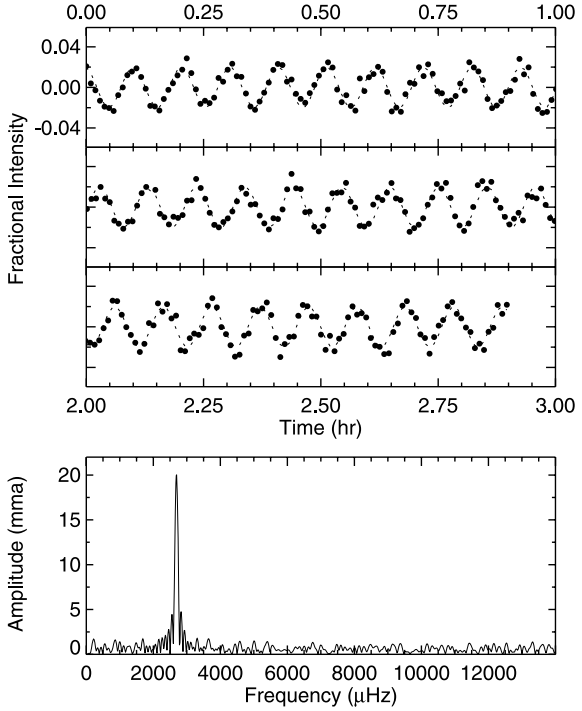

Figure 2. Top panel: sample light curve of CS 1246 from 2010 January 18. The data shown were obtained with the PROMPT 3 over 2.9 h using 30-s exposures without a filter. Bottom panel: amplitude spectrum of the light curve, which is dominated by a 371.7-s signal.

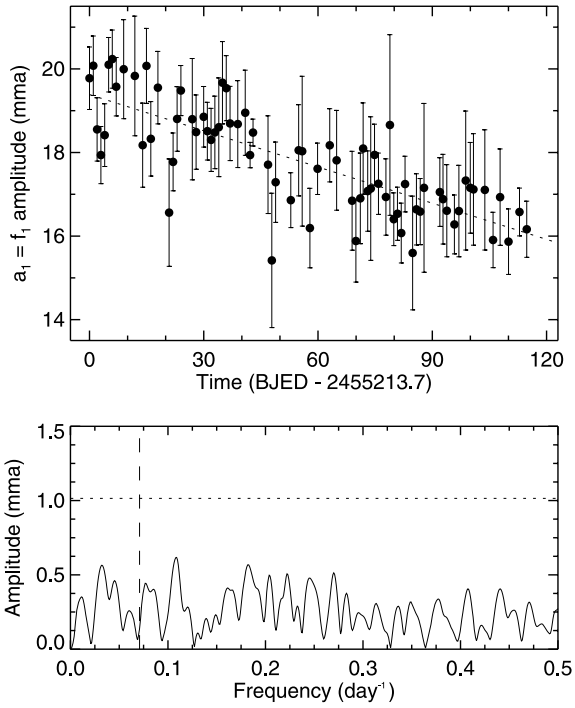

Figure 3. Top panel: amplitudes of f_1 taken from the least-squares fits to the individual 2010 light curves. The data show a decreasing trend of nearly 0.9 mma month^{-1}, which is marked by a dotted line. Bottom panel: FT of the nightly amplitudes with the linear trend removed. The mean noise level is 0.25 mma. The dashed vertical line marks the location of a 14.1-d oscillation and the dotted horizontal line represents the amplitude at four times the mean noise level.

& Breger 2005) and MPFIT (Markwardt 2009). Initially, the period, phase and amplitude were left as free parameters in the fits, but once we obtained a better determination of the period (see Section 3), we refitted all of the data with the period fixed. Fig. 2 shows a representative light curve from one of our photometry runs above its amplitude spectrum.

2.2 Night-by-night results

Each of the individual 89 light curves is dominated by the 371.7-s pulsation mode (hereinafter f_1) reported by Barlow et al. (2010) and shows no other significant signals in the p-mode range of the amplitude spectrum (1600–14 000 μHz) after pre-whitening the signal. Low-amplitude signals appear in some of the nightly Fourier transforms (FTs) at frequencies near the g-mode regime, but we hesitate to claim these signals as real since $1/f$ noise and improperly removed extinction effects could easily account for those structures.

Our least-squares fits show the amplitude of f_1 decreased from 20 mma[3] in 2010 January to 16 mma in 2010 May at a rate of nearly 0.9 mma month^{-1}. Fig. 3 presents this trend above its FT. We exclude the 2009 data from this plot since they were taken primarily through different passbands from the 2010 data and the measured amplitude of f_1 strongly depends on the observed wavelengths (Barlow et al. 2010). If the rate of decline remains linear, f_1 will have an amplitude below our detection limits (in nightly light curves) by 2011 November. As we discuss later, there is no detectable periodic signal in the amplitudes.

The frequencies of f_1 in all the light curves agree within their error bars, which were typically around 1.2 μHz. To investigate smaller changes in the frequency as well as variations in the phase, we analysed our complete data set using the O−C technique, as discussed in the section that follows.

3 THE O−C DIAGRAM

We began our construction of the O−C diagram[4] by calculating a linear ephemeris for the times of maxima in the light curve (C) of the form

$$C = T_c + P_c E, \quad (1)$$

where T_c is a reference time of maximum, P_c is the pulsation period and E is the cycle number measured from T_c. Since keeping track of E correctly over an extended period of time requires an exceptionally accurate starting frequency, we used the period resulting from the least-squares fits to the combined 2010 light curve for P_c. Our observing run on 2010 March 10 falls near the middle of this combined light curve and, consequently, we employed the time of maximum determined from its least-squares fit for T_c. The observed times of maxima (O) were taken from the least-squares fits to the individual light curves and their corresponding cycle numbers were computed using equation (1).

Fig. 4 presents the O−C diagram created by subtracting the calculated from the observed times of maxima. A sinusoidal oscillation dominates the overall structure. The sinusoid is superimposed on a

[3] Amplitudes are given in units of millimodulation amplitude (mma) or parts-per-thousand. 10 mma corresponds to 1 per cent.

[4] For a review of the basic principles behind the O−C method, we refer the reader to Kepler (1993).

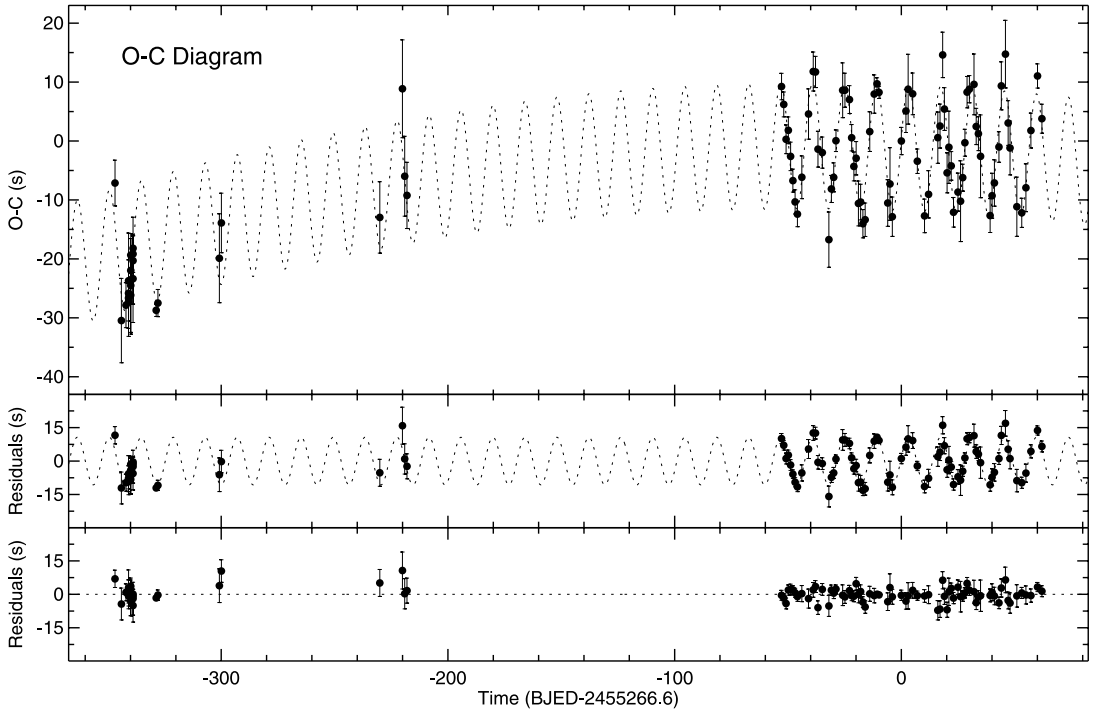

Figure 4. Top panel: the O−C diagram for CS 1246. O−C values were computed using f_1 and a linear ephemeris. The diagram is dominated by a strong sinusoidal pattern with a period of 14.1 d overlaid on a parabola. Middle panel: O−C points after the removal of the quadratic term. Bottom panel: O−C points after the removal of both the parabola and the sine wave. The mean noise level in the pre-whitened diagram is 0.75 s.

parabolic trend indicative of a secular change in the pulsation period. The presence of the sinusoid is even more apparent in the FT of the O−C diagram with the quadratic term removed, as shown in Fig. 5. To quantify these structures, we performed a simultaneous fit to the O−C values, including both parabolic and sinusoidal terms, using the expression

$$\mathrm{O-C} = \Delta T + \Delta P E + \frac{1}{2} P \dot{P} E^2 + A \sin\left(\frac{2\pi E}{\Pi} + \phi\right). \quad (2)$$

We used the IDL routine MPFIT (Markwardt 2009), which employs the Levenberg–Marquardt method, to perform a non-linear least-squares fit of equation (2) to the data. During this process, the points were weighted by their phase error bars as determined from the least-squares fits. Inspecting both equations (1) and (2), one finds that the resulting values for ΔT and ΔP provide corrections to our initial estimates for the reference time of maximum and period from which we derive a final pulsational ephemeris for the times of maxima:

$$t_{\max} = T_{\mathrm{O}} + P E + \frac{1}{2} P \dot{P} E^2 + A \sin\left(\frac{2\pi E}{\Pi} + \phi\right). \quad (3)$$

Table 1 displays the best-fitting parameters for this ephemeris.

The parabolic component of the fit indicates a secular decrease in the pulsational period of the order of 1 ms every 1.7 yr. We attribute this variation to structural changes in CS 1246 as it evolves, as we discuss further in Section 6. Removing this signal from the O−C data (Fig. 4, middle panel) more clearly reveals the two-week phase oscillation, which has a semiamplitude of nearly 11 s. We point out that even the 2009 data, which are separated from the 2010 points by more than five months, phase well to this oscillation. We find no additional phase variations after removing the parabolic and sinusoidal terms in either the O−C diagram (Fig. 4, bottom panel) or its FT (Fig. 5, bottom panel). The mean noise level in the FT of the pre-whitened O−C diagram is 0.75 s.

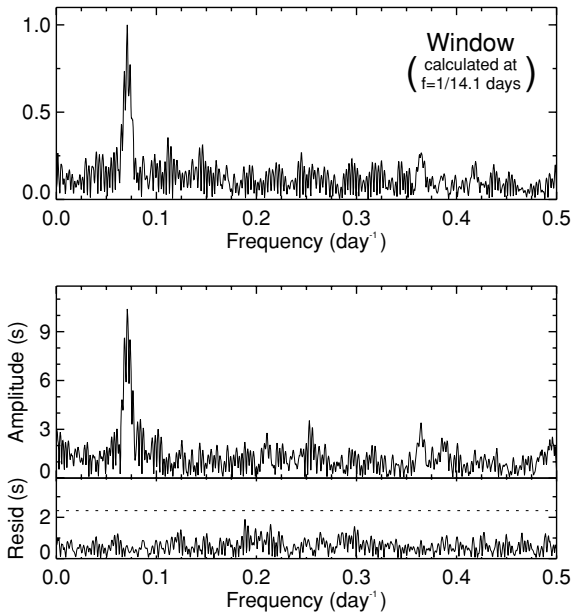

Figure 5. FT of the O−C values after the removal of the quadratic term (middle panel). For reference, the window function for a sine wave sampled in the same manner as our data is also shown (top panel). The FT of the data with the parabola and sine wave removed (bottom panel) has a mean noise level of 0.75 s. The dashed line marks the 4σ level.

4 THE COMBINED LIGHT CURVE

Three global variations associated with the pulsations of f_1 have been presented thus far: an amplitude decrease, a two-week phase

Table 1. Ephemeris parameters for the times of light maxima given in equation (3).

Parameter	Value	Error	Unit	Comment
T_O	2455 266.604 605	±0.000 004	d	Time of light maximum
P	371.691 62	±0.000 04	s	f_1 pulsational period[a]
$\dot{P}$	-1.9×10^{-11}	$\pm 0.3 \times 10^{-11}$	s s^{-1}	f_1 pulsational period change[a]
A	10.7	±0.4	s	Fortnightly phase-variation semiamplitude
Π	14.103	±0.010	d	Fortnightly phase-variation period
ϕ	0.023	±0.007	cycles	Fortnightly phase-variation phase[a]

[a]As measured at T_O.

oscillation and a decrease in the pulsation period. Each of these phenomena should manifest itself in the FT of the combined light curve in a particular way. For this reason and to look for lower amplitude signals not detectable in the nightly light curves, we combined the light curves and computed the FT of the result. The 2009 light curves were ignored in this analysis since they are few in number compared to the 2010 data and the large gaps they introduce to the combined light curve overly complicate the window function.

Fig. 6(a) shows the amplitude spectrum of the complete light curve with an expanded view around f_1, which clearly dominates the spectrum. After removing a sine wave of fixed frequency and amplitude from the light curve and recomputing the FT (Fig. 6b), one can see significant power at the location of the first harmonic of the main mode (5381 μHz) with an amplitude near 0.6 mma. The probability that random noise could produce this much signal by chance at exactly $2f_1$ is less than 10^{-12}; consequently, we regard this signal as real. Evaluating the amplitude spectra of light curves combined month by month provides further support for the presence of the first harmonic.

Even more prominent than the first harmonic, the amplitude spectrum of the pre-whitened light curve reveals a substantial amount of residual structure surrounding the location of f_1. The most significant of these signals is an apparent 0.82-μHz splitting of f_1 and its sidelobes, which is shown in the right half of Fig. 6(b). With an amplitude nearly 10 per cent that of the original mode, these components are split by exactly 1/14.1 d, corresponding to the period of the phase oscillation observed in the O−C diagram. An additional splitting with an even tighter frequency separation and much smaller amplitude is also visible in the panel.

To test whether the above structures are consistent with the aforementioned three global variations associated with f_1, we modelled

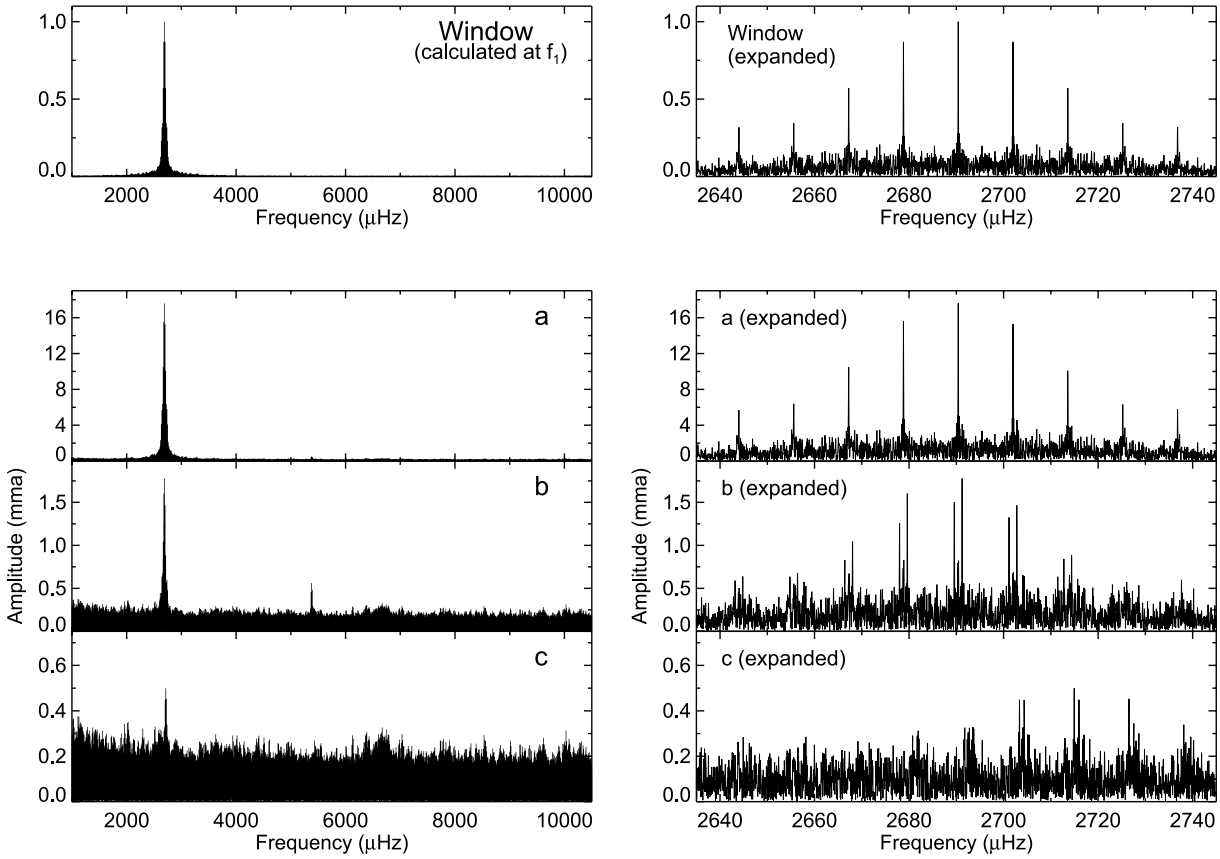

Figure 6. (a) Amplitude spectrum of the combined 2010 light curve (left-hand column) with expansions around f_1 (right-hand column). (b) Spectrum of the light curve pre-whitened by a sine wave with frequency f_1, which reveals a 0.82-μHz splitting of f_1. Note also the presence of the first harmonic to f_1. (c) Amplitude spectrum of the data pre-whitened by the best fit of equation (4). The mean noise level is around 0.074 mma.

Table 2. Best-fitting parameters to equation (4).

Parameter	Value	Error	Unit	Comment
a_1	17.71	±0.075	mma	f_1 amplitude[a]
$\dot{a}_1$	−0.0298	±0.0027	mma d^{-1}	f_1 amplitude change[b]
a_2	0.5858	±0.075	mma	$2f_1$ amplitude[a,c]
P	371.691 646	±0.000 033	s	f_1 period[a]
$\dot{P}$	−1.88	(fixed)	10^{-11} s s^{-1}	f_1 period change[d]
A	10.69	±0.35	s	f_1 phase-oscillation semiamplitude
Π	14.067	±0.032	d	f_1 phase-oscillation period
ϕ_1	0.856 54	±0.000 70	cycles	f_1 phase[a]
ϕ_2	0.435	±0.020	cycles	f_2 phase[a]
ϕ_π	0.8456	±0.0055	cycles	Phase of the f_1 phase oscillation[a]

[a]At $t = 0$ corresponding to BJED 245 5271.197436.
[b]From 2010 January to May.
[c]With f_2 fixed to $2f_1$.
[d]Fixed to a value from Table 1.

the complete light curve with the function

$$I(t) = (a_1 + \dot{a}_1 t)\sin\left[\frac{2\pi t}{P + \dot{P}t} + \phi_1 + \phi(t)\right] + a_2 \sin\left[\frac{2\pi t}{\frac{P}{2} + \frac{\dot{P}}{2}t} + \phi_2 + 2\phi(t)\right], \quad (4)$$

which includes a fundamental mode and the first harmonic with linear period changes. Additionally, the fundamental mode is given a linear amplitude variation. Both terms contain a phase oscillation given by

$$\phi(t) = \frac{2\pi A}{P + \dot{P}t}\sin\left(\frac{2\pi t}{\Pi} + \phi_\pi\right). \quad (5)$$

Fixing $\dot{P}$ to its value determined from the O−C diagram, we let all other parameters vary freely and used MPFIT to find the best-fitting values shown in Table 2. We note that all fitted parameters determined previously in this manuscript ($P, A, \Pi, \dot{a}_1, a_1, a_2$) using other methods (O−C diagram, night-by-night light-curve fits) agree with those in the table to within the errors. Subtracting this fit from the data and recalculating the FT (Fig. 6c) shows that our model removed essentially all of the signals centred around f_1. The only signal remaining in the amplitude spectrum after this process is a low-amplitude peak offset by 15 μHz from f_1 at 2715 μHz. The frequency separation from f_1 implies an interaction time-scale of 0.5 d. The origin of this signal is unclear, but the probability that noise could produce it by chance is less than 10^{-5}.

Other scenarios could also lead to the residual FT structure observed around f_1 in Fig. 6(b), but they would have to do by conspiracy what our proposed model does naturally. The equidistant triplets might be produced by (i) the splitting of f_1 by stellar rotation; (ii) the presence of additional independent pulsation frequencies symmetrically disposed of about the original; (iii) one independent pulsation frequency and a combination mode at the difference between it and the first harmonic; and (iv) the amplitude variability of f_1. None of these is appealing nor as effective as the model of equation (4) at removing the residual power. In particular, all of the alternative models predict an amplitude modulation of f_1 with a period of two weeks, which is not seen in the FT of the amplitude fits after the decreasing amplitude trend is removed (Fig. 3, bottom panel).

5 BINARY SYSTEM PARAMETERS

Under the assumption that the O−C variations represent the reflex motion due to an orbital companion, we have fitted the best orbital parameters. Using the fits in Table 1, CS 1246 moves about a barycentre at least 11 light-seconds (4.7 $R_\odot$) away with a period of two weeks. If the orbit is perfectly circular, the phase variation will be sinusoidal; otherwise, the shape will deviate from a sine wave. As some subdwarf binaries show small eccentricities in their orbits (Edelmann, Altmann & Heber 2006), we decided to evaluate the eccentricity of the orbit by investigating both the phase-folded O−C curve and the FT thereof. Fig. 7 presents the phase-folded O−C diagram after the removal of the parabolic trend.

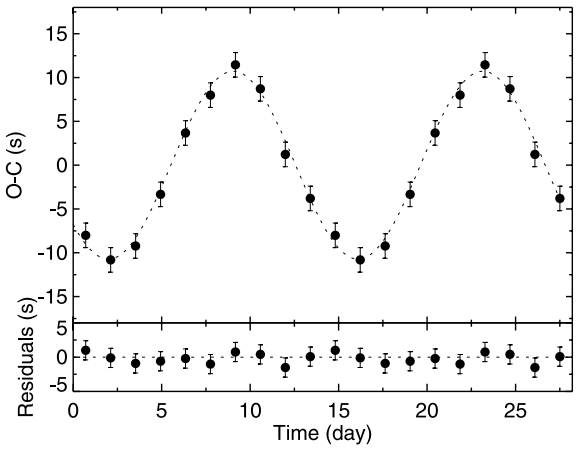

Figure 7. Top panel: phase-folded O−C diagram with the parabola removed. The O−C points were folded on the fortnightly periodicity and averaged into 10 bins. The dotted line shows the circular orbit fit to the O−C diagram. Bottom panel: residual O−C values after the removal of a sinusoid fit.

The best-fitting orbital parameters to the folded O−C diagram yield an eccentricity of $\epsilon = 0.04 \pm 0.04$, which we take to be consistent with a circular orbit. The absence of a prominent first harmonic (at 0.14 d^{-1}) in the FT of the O−C diagram (Fig. 5, bottom panel), which would be expected for a considerably elliptical orbit, corroborates this conclusion. Some degree of eccentricity might be expected since the circularization time-scale for a binary with a two-week orbital period exceeds 2 billion years (Tassoul & Tassoul 1992) but would not significantly alter the results of our mass determination.

Without information concerning the orbital motion of the unseen companion, we are limited to computing the mass function for the

Table 3. System parameters.

Parameter	Value	Error	Unit	Comment
Π	14.105	$\pm$0.011	d	Orbital period
K	16.6	$\pm$0.6	km s^{-1}	RV semiamplitude[a]
f	0.0066	$\pm$0.0007	$M_\odot$	Mass function
a	0.0910	$\pm$0.0003	au	Separation distance[b]
	0.0963	$\pm$0.0003	au	Separation distance[c]
$m \sin i$	0.115	$\pm$0.005	$M_\odot$	Minimum companion mass[b,d]
	0.129	$\pm$0.005	$M_\odot$	Minimum companion mass[c,d]

[a]Circular orbit approximation.
[b]Assuming an sdB star mass of 0.39 $M_\odot$
[c]Assuming a canonical sdB star mass of 0.47 $M_\odot$
[d]Assumes no error bar on the sdB star mass.

system:

$$f = \frac{m^3 \sin^3 i}{(m+M)^2} = \frac{PK^3}{2\pi G}. \quad (6)$$

The companion mass (m), sdB mass (M) and inclination angle (i) are free parameters, while the period (P) and RV semiamplitude (K) of the sdB star are taken from our fits to the O−C diagram. To compute the mass of the companion, we must assume a mass for the sdB star. Barlow et al. (2010) showed that under the assumption of a radial oscillation, a mass of $0.39^{+0.30}_{-0.13}\,M_\odot$ could be derived using the Baade–Wesselink method. However, since the error bars are large and the radial nature of f_1 remains unproven, we use both this mass and the canonical sdB star mass (0.47 $M_\odot$; Han et al. 2002, 2003) to derive the system parameters shown in Table 3.

The minimum mass derived for the unseen companion is 0.12 $M_\odot$. Further limitations could be placed on this mass by constraining the inclination angle of the system. If the orbital plane is nearly edge-on ($i \simeq 90^\circ$), primary and secondary eclipses will occur when the O−C variations are close to their maximum and minimum values, respectively. To look for an eclipse, we carefully monitored the light curve using three of the PROMPT on 2010 June 21 (UTC) at a time when equation (3) predicts a primary eclipse of the sdB star in the case of an edge-on orbital plane. None of the light curves showed any sign of a signal loss. Given the large separation distance, the absence of an eclipse only rules out inclination angles greater than 89°, which increases the minimum mass we report by a negligible amount.

Under the assumption of randomly distributed orbital plane orientations, one computes the probability of observing a system at an inclination angle i less than or equal to θ as

$$\text{Probability} : (i < \theta) = 1 - \cos\theta. \quad (7)$$

From this we calculate a 96 per cent probability that the companion mass is less than 0.45 $M_\odot$; hence, the object is most likely a low-mass white dwarf or late-type main-sequence M dwarf. Optical spectra of CS 1246 (Barlow et al. 2010) show no clear signatures of a companion, but this result is consistent with both companion possibilities. Optical reflection effects are often observed in sdB+dM systems, but even if the albedo of the M dwarf were 1.0, the relatively large separation distance would result in a maximum flux increase less than 0.01 mma, a modulation well below our detection limits. An infrared excess would be expected for CS 1246 if the companion is a main-sequence star with mass exceeding 0.45 $M_\odot$ (Lisker et al. 2005). Unfortunately, the presence of the Coalsack Nebula along our line of sight significantly reddens the system flux and complicates the identification of an infrared excess from a companion.

6 THE EVOLUTION OF CS 1246

Clues to the current evolutionary state of CS 1246 may be found through the consideration of the pulsational $\dot{P}$. According to the models of Charpinet et al. (2002), changes in the periods of acoustic modes in EHB stars are dominated by two primary phases. During the first, a decrease in the surface gravity causes the periods to increase steadily as the sdB star evolves away from the zero-age extended horizontal branch (ZAEHB). Model stars display positive values of $\dot{P}$ in this phase. The second phase of evolution begins approximately 90 Myr after the ZAEHB when the density of the thermonuclear fuel in the core begins to decrease dramatically. Responding to the reduced energy production, the model stars contract and the resultant increase in surface gravity leads to a decrease in acoustic mode periods and hence a negative value for $\dot{P}$. This phase lasts until the onset of the post-EHB phase approximately 110 Myr after the ZAEHB, at which point He in the core is completely exhausted. Thereafter, He fusion may begin in the shell, the radius begins to increase and the star heads towards the white dwarf cooling sequence after passing through the subdwarf O (sdO) regime of the H–R diagram. Most helium-deficient sdO stars are believed to be the progeny of sdB stars evolving in this way.

Our negative value of $\dot{P}$, interpreted as an evolutionary effect, implies CS 1246 is nearing the end of its life as an EHB star or has already done so. The contraction resulting from the depletion of He in the core yields an increased surface gravity, which leads to a decrease in the pulsational period of -571 ± 85 s Myr^{-1}. Charpinet et al. (2002) calculated values of $\dot{P}$ for sdB star acoustic modes (their appendix C) for representative models at different ages. Comparing our $\dot{P}$ to all of their theoretical ones, we find our rate of change to be more rapid than all of their listed values but most closely matches that of a radial mode in a model with an age of 106.58 Myr and a hydrogen layer mass of 0.0042 $M_\odot$. Our faster $\dot{P}$ could result from CS 1246 having a thicker hydrogen layer than any of their models, since Charpinet et al. (2002) show that increasing the hydrogen layer mass leads to faster period changes. It is also possible that CS 1246 exists in an evolutionary epoch not represented in their table. Charpinet et al. (2002) note that in advanced stages of EHB evolution, when the period decreases most rapidly, they used simple forward differencing to estimate theoretical $\dot{P}$ values instead of cubic spline fittings, which they used in earlier EHB stages when the periods are more stable. A potential consequence of this differencing is the over- or under-estimation of period changes at these advanced evolutionary stages.

Having stated these possibilities, we stress that our measurement of $\dot{P}$ is at most an *upper limit* to the evolutionary rate of CS 1246. Secular processes in sdB stars work on slower time-scales than other processes affecting the phase or frequency of a mode, which in some cases drive the observed $\dot{P}$ to faster changes (Kawaler 2010). Proper motion, for example, can contribute to the measured period changes in pulsating stars (Pajdosz 1995), but the expected contribution in our case is several orders of magnitude smaller than our observed $\dot{P}$ and inconsequential to our analysis.

7 DISCUSSION AND OUTLOOK

Using the O−C technique, we have discovered an apparent orbital reflex motion in CS 1246 and measured an upper limit of $\dot{P}$ for its main pulsation mode. This marks the second time such quantities have been derived for an sdBV star using this method. The first measurements were from Silvotti et al. (2007). The measured rate of period change, if secular, implies that the star has either already exhausted the He in its core or is quickly approaching the

post-EHB stage. Models show that the structure of sdB stars in this evolutionary state changes dramatically fast and it may even be possible to measure $\ddot{P}$ within a few years.

An analysis using Kepler's law shows that the companion has a minimum mass near $0.12\,M_{\odot}$ and is most likely a white dwarf or late-type main-sequence star. The separation distance implies that the companion was potentially inside the envelope of the sdB progenitor during its red giant phase and might even be responsible for the ejection of the envelope (see Han et al. 2002, 2003). We cannot rule out the presence of additional bodies in the system, but we can limit the possible combinations of companion masses and separation distances using the detection limits from the FT of our O−C data. The shaded region in Fig. 8 shows combinations of masses and separation distances leading to phase wobbles that are *undetectable* using our current data set. Our ability to detect a companion with orbital parameters inside the white region depends on the inclination angle of its orbit. The lower solid line shows the combinations of system parameters resulting in reflex motions equal to our detection limits, under the assumption of an edge-on orbital plane; the line moves up with increasing inclination angle. The region is bounded on the left-hand side and right-hand side by the dashed lines corresponding to the minimum and maximum orbital periods we can detect, given the sampling rate and baseline of our O−C data; thus, we could expand the area of the white region by obtaining phase measurements more frequently or by monitoring the system for a longer period of time. Regardless of the sampling, additional phase measurements will lower our detection limits and move the lower boundary (solid line) to smaller masses. As a reference, the star symbol shows the location of the single companion we detect around CS 1246 (plotted with its minimum mass). If the observed phase oscillation is the result of a binary companion, CS 1246 would show the second-lowest RV semiamplitude and the third-longest period of the ∼85 sdB binary systems for which orbital parameters are known (table A.1, Geier et al. 2011).

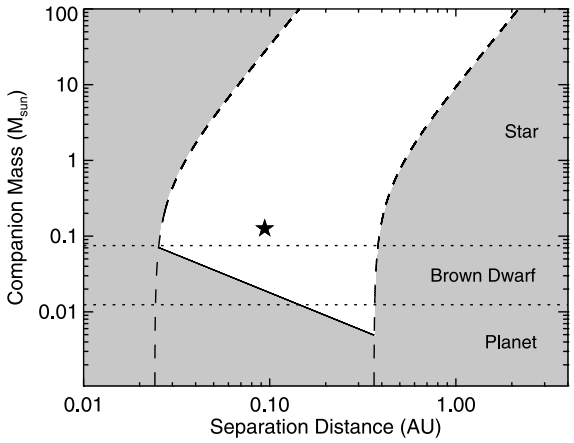

Figure 8. Approximate sensitivity of our O−C diagram to companions around CS 1246. The shaded region marks objects that are *not* detectable using the O−C data shown in Fig. 4. Companions falling within the white region could be detected in our data set, with certain restrictions on their orbital inclination angle. For these calculations, we assume a mass of $0.47\,M_{\odot}$ for CS 1246. The two dashed lines mark the combinations of companion masses and separation distances leading to orbital periods equal to the longest (right-hand dashed line) and shortest (left-hand dashed line) periods detectable using our O−C data, as computed using Kepler's third law. The solid line shows the combinations of masses and distances resulting in reflex motions equal to our detection limits in the FT of the O−C diagram, under the assumption of an edge-on orbital plane. Masses below this line induce reflex motion below our detection limits, regardless of their inclination angles. The star symbol marks the location of the companion we detected (plotted using the minimum mass) and the two dotted horizontal lines show the boundaries between the planet and brown dwarf masses (lower dotted line) and between the brown dwarf and stellar masses (upper dotted line).

More statistics are needed to draw conclusions about the formation channels leading to sdB stars from the orbital parameters of binary systems. Searches for RV variations, as are being carried out by the MUCHFUSS (Geier et al. 2011), should uncover a wide variety of sdB binary systems, although they are somewhat biased towards higher mass systems with shorter orbital periods. Pulsating sdB stars may also be used to find unseen companions using the O−C diagram, as shown in this work and by Silvotti et al. (2007), and the EXOTIME project (Schuh et al. 2010) is currently building up O−C diagrams for several sdBV stars to look for oscillations in the pulse timings. Although both these surveys will be effective at uncovering binary companions to sdB stars, their sampling rates differ significantly from the one presented in this study and, consequently, they will not be sensitive to the same parameter space as shown in Fig. 8.

Our result provides an important link between the two aforementioned methods for detecting unseen companions since an observable RV variation should accompany our fortnightly phase oscillation. The O−C diagram is a significant tool used to discover and characterize the nature of unseen companions, including extrasolar planets, but no corroborative RV variations have been measured to date. The O−C oscillation of CS 1246 implies a two-week velocity variation with a semiamplitude well within the range of medium- to high-resolution spectrographs. Consequently, we are planning follow-up observations to measure the RV variations. If the expected RV variation is observed, it will be the first independent confirmation that it is possible to detect stellar and planetary companions using the O−C technique with sdB pulsations as the clock.

ACKNOWLEDGMENTS

We acknowledge the support of the National Science Foundation, under award AST-0707381, and are grateful to the Abraham Goodman family for providing the financial support that made the spectrograph possible. BNB acknowledges additional support from a GAANN fellowship, Department of Education award number P200A090135. We thank the Delaware Asteroseismic Research Center for providing the *S*8612 filter used in these studies. We also recognize the observational support provided by the SOAR telescope operators Alberto Pasten, Patricio Ugarte, Sergio Pizarro and Daniel Maturana. The SOAR telescope is operated by the Association of Universities for Research in Astronomy, Inc., under a cooperative agreement between the CNPq, Brazil, the National Observatory for Optical Astronomy, the University of North Carolina and Michigan State University, USA.

REFERENCES

Barlow B. N. et al., 2010, MNRAS, 403, 324
Charpinet S., Fontaine G., Brassard P., Dorman B., 1996, ApJ, 471, L103
Charpinet S., Fontaine G., Brassard P., Chayer P., Rogers F. J., Iglesias C. A., Dorman B., 1997, ApJ, 483, L123
Charpinet S., Fontaine G., Brassard P., Dorman B., 2002, ApJS, 140, 469
Clemens J. C., Crain J. A., Anderson R., 2004, in Moorwood A. F. M., Iye M., eds, Proc. SPIE Vol. 5492, Ground-based Instrumentation for Astronomy. SPIE, Bellingham, p. 331
D'Cruz N. L., Dorman B., Rood R. T., O'Connell R. W., 1996, ApJ, 466, 359
Edelmann H., Altmann M., Heber U., 2006, Balt. Astron., 15, 191

Geier S. et al., 2011, A&A, in press (arXiv:1103.4045)
Han Z., Podsiadlowski P., Maxted P. F. L., Marsh T. R., Ivanova N., 2002, MNRAS, 336, 449
Han Z., Podsiadlowski P., Maxted P. F. L., Marsh T. R., 2003, MNRAS, 341, 669
Heber U., 1986, A&A, 155, 33
Kawaler S. D., 2010, Astron. Nachr., 331, 1020
Kepler S. O., 1993, Balt. Astron., 2, 515
Kilkenny D., Koen C., O'Donoghue D., Stobie R. S., 1997, MNRAS, 285, 640
Kilkenny D., Fontaine G., Green E. M., Schuh S., 2010, Inf. Bull. Var. Stars, 5927, 1
Lenz P., Breger M., 2005, Commun. Asteroseismol., 146, 53
Lisker T., Heber U., Napiwotzki R., Christlieb N., Han Z., Homeier D., Reimers D., 2005, A&A, 430, 223
Markwardt C. B., 2009, in Bohlender D. A., Durand D., Dowler P., eds, ASP Conf. Ser. Vol. 411, Astronomical Data Analysis Software and Systems (ADASS) XVIII. Astron. Soc. Pac., San Francisco, p. 251
Maxted P. f. L., Heber U., Marsh T. R., North R. C., 2001, MNRAS, 326, 1391
Morales-Rueda L., Maxted P. F. L., Marsh T. R., North R. C., Heber U., 2003, MNRAS, 338, 752
Napiwotzki R., Karl C. A., Lisker T., Heber U., Christlieb N., Reimers D., Nelemans G., Homeier D., 2004, Ap&SS, 291, 321
Østensen R. H., 2009, Commun. Asteroseismol., 159, 75
Pajdosz G., 1995, in Stobie R. S., Whitelock P. A., eds, IAU Colloq. 155, ASP Conf. Ser. Vol. 83, Astrophysical Applications of Stellar Pulsation. Astron. Soc. Pac., San Francisco, p. 439
Reichart D. et al., 2005, Nuovo Cimento C Geophys. Space Phys. C, 28, 767
Schuh S. et al., 2010, Ap&SS, 329, 231
Silvotti R. et al., 2007, Nat, 449, 189
Soker N., 1998, AJ, 116, 1308
Stumpff P., 1980, A&AS, 41, 1
Tassoul J., Tassoul M., 1992, ApJ, 395, 259
Thompson S. E., Mullally F., 2009, J. Phys. Conf. Ser., 172, 012081

APPENDIX A: O−C POINTS

Table A1. Observation log.

Date (UTC)	Start time (UTC)	T_{exp} (s)	T_{cycle} (s)	Length (h)	Filter	Telescope[a]	Date (UTC)	Start time (UTC)	T_{exp} (s)	T_{cycle} (s)	Length (h)	Filter	Telescope[a]
2009-03-29	05:13:09	40	46	1.23	*V*	P4	2010-02-21	02:00:07	30	36	2.91	Open	P3
2009-04-01	00:51:02	40	46	1.40	*V*	P5	2010-02-22	02:07:14	30	36	2.41	Open	P3
2009-04-03	01:16:16	20	26	1.17	Open	P4	2010-02-23	01:52:20	31	37	2.48	Open	P3
2009-04-03	23:59:03	80	86	9.43	u'	P3	2010-02-25	02:27:30	30	36	2.40	Open	P3
2009-04-04	00:57:03	40	52	9.57	g'	P2	2010-02-27	01:37:09	30	36	3.11	Open	P3
2009-04-04	00:01:48	40	47	9.57	r'	P4	2010-02-28	08:04:58	20	26	1.78	*S*8612	SOAR
2009-04-04	00:01:52	40	47	8.66	i'	P5	2010-03-01	02:37:10	20	26	6.79	*B*	SOAR
2009-04-04	23:57:56	80	86	8.61	u'	P3	2010-03-05	01:13:28	30	36	2.41	Open	P3
2009-04-04	23:57:06	40	52	9.31	g'	P2	2010-03-06	01:09:45	30	36	1.61	Open	P3
2009-04-04	23:57:42	40	47	9.29	r'	P4	2010-03-07	01:06:47	30	36	2.92	Open	P3
2009-04-04	23:57:39	40	47	9.43	i'	P5	2010-03-11	00:44:23	30	36	3.20	Open	P3
2009-04-05	23:56:42	80	86	9.70	u'	P3	2010-03-13	02:09:46	30	36	1.64	Open	P3
2009-04-05	23:55:47	40	52	9.69	g'	P2	2010-03-14	00:32:23	30	36	3.19	Open	P3
2009-04-05	23:56:36	40	47	9.68	r'	P4	2010-03-16	01:00:50	30	36	2.59	Open	P3
2009-04-05	23:56:32	40	47	9.69	i'	P5	2010-03-18	01:21:58	30	36	4.37	Open	P3
2009-04-16	09:07:06	10	16	1.10	*R*	SOAR	2010-03-21	06:02:18	30	36	3.41	Open	P3
2009-04-17	01:00:22	80	86	6.14	350–620 nm[b]	SOAR	2010-03-23	01:20:24	30	36	2.56	Open	P3
2009-05-14	05:09:12	20	26	3.08	*V*	P5	2010-03-27	03:00:52	30	36	2.14	Open	P3
2009-05-15	00:57:56	20	26	5.45	*V*	P5	2010-03-28	02:51:33	30	36	1.71	Open	P3
2009-07-23	23:36:05	40	46	3.25	*V*	P4	2010-03-29	06:30:50	30	36	2.99	Open	P3
2009-08-02	23:35:20	40	46	2.67	r'	P3	2010-03-30	00:28:42	30	36	3.00	Open	P3
2009-08-04	00:00:41	40	46	1.48	r'	P3	2010-03-31	05:06:29	30	36	2.99	Open	P3
2009-08-05	00:00:48	40	46	2.12	r'	P3	2010-04-01	00:29:16	30	36	1.98	Open	P3
2010-01-17	04:18:07	30	36	3.25	Open	P3	2010-04-02	00:17:15	30	36	3.97	Open	P3
2010-01-18	04:13:15	30	36	2.90	Open	P3	2010-04-03	00:50:48	30	36	3.49	Open	P3
2010-01-19	04:09:46	30	36	3.88	Open	P3	2010-04-04	23:58:13	30	36	3.08	Open	P3
2010-01-20	04:05:29	30	36	3.94	Open	P3	2010-04-06	01:26:05	30	36	7.95	Open	P3
2010-01-21	04:01:50	30	36	3.90	Open	P3	2010-04-07	00:46:28	30	36	5.28	Open	P3
2010-01-22	04:52:00	33	39	2.91	Open	P3	2010-04-08	00:41:50	30	36	4.67	Open	P3
2010-01-23	03:53:38	25	31	3.38	Open	P3	2010-04-09	00:42:05	30	36	2.98	Open	P3
2010-01-24	04:39:12	30	36	3.42	Open	P3	2010-04-10	00:38:21	30	36	3.59	Open	P3
2010-01-26	03:42:18	30	36	1.48	Open	P3	2010-04-12	00:12:12	30	36	5.56	Open	P3
2010-01-29	01:51:06	30	36	3.74	Open	P3	2010-04-13	00:07:47	30	36	4.99	Open	P3
2010-01-31	03:22:26	30	36	3.93	Open	P3	2010-04-14	00:03:33	30	36	3.70	Open	P3
2010-02-01	03:18:25	30	36	4.96	Open	P3	2010-04-15	00:03:48	30	36	1.90	Open	P3
2010-02-02	06:41:19	30	36	1.93	Open	P3	2010-04-19	03:51:05	30	36	4.29	Open	P3
2010-02-04	03:06:53	30	36	4.59	Open	P3	2010-04-19	23:49:39	30	36	5.41	Open	P3
2010-02-07	01:56:24	30	36	2.69	Open	P3	2010-04-20	23:39:39	30	36	7.40	Open	P3
2010-02-08	04:19:12	30	36	5.38	Open	P3	2010-04-22	23:37:12	30	36	6.63	Open	P3
2010-02-09	04:00:47	30	36	3.84	Open	P3	2010-04-24	03:47:37	30	36	1.84	Open	P3
2010-02-10	04:01:02	30	36	4.04	Open	P3	2010-04-25	22:58:30	30	36	2.82	Open	P3
2010-02-13	03:49:45	30	36	2.55	Open	P3	2010-04-27	03:31:02	30	36	3.66	Open	P3

Table A1 – *continued*

Date (UTC)	Start time (UTC)	T_{exp} (s)	T_{cycle} (s)	Length (h)	Filter	Telescope[a]	Date (UTC)	Start time (UTC)	T_{exp} (s)	T_{cycle} (s)	Length (h)	Filter	Telescope[a]
2010-02-14	03:59:15	30	36	2.33	Open	P3	2010-04-27	23:33:40	30	36	2.50	Open	P3
2010-02-16	03:51:20	30	36	2.33	Open	P3	2010-04-30	23:16:38	30	36	3.58	Open	P3
2010-02-17	02:49:32	30	36	3.00	Open	P3	2010-05-03	02:56:35	30	36	4.16	Open	P3
2010-02-18	02:11:52	30	36	3.11	Open	P3	2010-05-04	23:28:40	30	36	3.11	Open	P3
2010-02-19	02:08:17	30	36	3.23	Open	P3	2010-05-07	04:31:20	30	36	2.92	Open	P3
2010-02-20	02:58:25	30	36	2.21	Open	P3	2010-05-10	23:23:16	30	36	4.15	Open	P3

[a] 'P' = PROMPT.
[b] Light curve produced from time-series spectra over the wavelength range 3500–6200 Å.

Table A2. Observed times of light maxima and corresponding O−C values.

Time of maximum (BJED −245 0000)	Error (s)	O−C (s)	Time of maximum (BJED −245 0000)	Error (s)	O−C (s)
4919.752522	±3.9	−7.1	5248.652306	±3.0	−10.4
4922.574358	±7.2	−30.5	5249.646023	±2.4	−14.0
4924.587722	±3.8	−27.8	5250.635488	±2.8	−13.4
4925.701949	±6.5	−26.7	5252.661896	±3.4	1.6
4925.714875	±1.8	−25.8	5254.640884	±3.3	8.0
4925.714857	±3.2	−27.3	5255.879877	±1.0	9.7
4925.732098	±8.1	−23.7	5256.757465	±1.0	8.3
4926.682811	±6.6	−26.2	5260.607526	±4.0	−10.5
4926.700089	±3.7	−19.4	5261.584115	±6.2	−7.3
4926.700058	±2.1	−22.0	5262.616527	±3.3	−12.8
4926.704334	±8.0	−24.5	5266.604618	±2.3	0.0
4927.698121	±7.4	−23.4	5268.630913	±3.6	5.1
4927.711063	±3.1	−19.2	5269.598903	±5.9	8.8
4927.711074	±2.1	−18.2	5271.603620	±3.5	8.0
4927.698156	±7.4	−20.3	5273.655536	±2.1	−3.4
4937.910976	±1.1	−28.7	5276.830294	±2.8	−12.7
4938.681036	±2.3	−27.5	5278.615661	±4.0	−9.0
4965.787953	±7.5	−19.9	5282.681150	±4.4	0.6
4966.665615	±5.1	−13.9	5283.662026	±3.7	2.5
5036.555718	±6.1	−13.0	5284.845213	±3.9	14.6
5046.545184	±8.3	8.9	5285.593652	±3.6	5.4
5047.538762	±6.8	−6.0	5286.785176	±3.4	−5.4
5048.549697	±5.6	−9.2	5287.572491	±6.1	−1.1
5213.750512	±2.2	9.2	5288.604931	±2.4	−4.2
5214.739933	±2.1	6.2	5289.615806	±2.5	−12.1
5215.759436	±2.4	0.3	5291.573250	±3.2	−8.7
5216.757515	±2.3	1.8	5292.726167	±6.9	−10.2
5217.755525	±2.4	−2.6	5293.676951	±2.3	−6.2
5218.770747	±1.9	−6.7	5294.636362	±2.3	−0.3
5219.738651	±2.1	−10.3	5295.600108	±2.7	8.3
5220.771104	±2.1	−12.4	5296.611080	±2.3	8.8
5222.715675	±3.6	−6.2	5298.654533	±5.2	9.6
5225.662660	±4.3	4.6	5299.618096	±3.1	2.5
5227.727697	±3.3	11.8	5300.594632	±2.9	1.2
5228.747268	±2.6	11.7	5301.549629	±7.0	−2.6
5229.826914	±3.0	−1.4	5305.761159	±2.9	−12.6
5231.732689	±2.6	−2.0	5306.617291	±3.8	−9.3
5234.644963	±4.7	−16.7	5307.649793	±3.9	−7.1
5235.754975	±2.3	−8.1	5309.663194	±2.6	−1.0
5236.765965	±2.5	−6.2	5310.708696	±4.1	9.4
5237.759795	±1.8	0.0	5312.524198	±5.7	14.7
5240.719663	±4.7	8.6	5313.711413	±3.8	3.1
5241.722024	±2.9	8.6	5314.541647	±4.6	−1.2
5243.718128	±2.4	7.0	5317.557226	±5.0	−11.1
5244.686000	±2.2	0.6	5319.721109	±2.5	−12.2
5245.662495	±2.5	−4.3	5321.562408	±4.1	−7.9
5246.664874	±2.8	−2.9	5323.760837	±3.0	1.8
5247.675753	±3.8	−10.6	5326.669086	±2.0	11.0

This paper has been typeset from a TEX/LATEX file prepared by the author.